The effect of the magnetic free energy on the phase stability at the Co-rich end of the Co-Cu binary system

1990 J. Phys.: Condens. Matter 2 5787

(http://iopscience.iop.org/0953-8984/2/26/016)

J. Phys.: Condens. Matter **2** (1990) 5787–5795. Printed in the UK

The effect of the magnetic free energy on the phase stability at the Co-rich end of the Co–Cu binary system

L H Chen†, M P Hung† and T S Chin‡

† Department of Materials Engineering, National Cheng Kung University, Tainan 70100, Taiwan, Republic of China

‡ Department of Materials Science and Engineering, National Tsing Hua University, Hsinchu 30043, Taiwan, Republic of China

Received 28 December 1989, in final form 20 March 1990

Abstract. The solvus phase boundaries of the Co–Cu system were recalculated by taking into account the effect of copper on the magnetic free energy of α-Co. It was confirmed that the solubility of copper in α-Co is significantly lowered owing to the magnetic ordering energy below the Curie temperature T_C and there is an anomaly in the Arrhenius plot of solubility. The precision lattice parameter determination by x-ray diffractometry and the intrinsic coercivity H_{ci} measurement by SQUID were performed and the calculated results were justified. Two different thermodynamic treatments of magnetic free energy were also compared in this study.

1. Introduction

The influence of magnetism on the phase stability was first pointed out by Zener [1]. He explained the abnormal shape of a γ-phase field curve in the Fe–Cr system as due to the magnetic ordering of iron. There were many such studies extending his idea and dividing the thermodynamic functions into magnetic and non-magnetic parts [2–6]. Nishizawa and co-workers [7, 8] have given a detailed description of the functions of magnetic free energy and succeeded in calculating the phase diagrams by considering the magnetic energy.

Another treatment of magnetic energy was presented by Hillert *et al* [9]. They correlated the magnetic free energy of alloys to the magnetic moment and Curie temperature T_C of each element. Later, Chuang *et al* [10–12] gave a simpler formulation of magnetic free energy and calculated the Fe–X binary phase diagrams.

Calculation of the Co–Cu phase diagram using the formulation of Nishizawa and co-workers has been carried out [8]. However, there are still some discrepancies between the experimental and calculated results of solubility curves in the Co-rich region. In order to reanalyse the solubility of Cu in α-Co, the magnetic free energy was incorporated into the calculation of the solubility using the formulation proposed by Chuang *et al* [10], and experiments were also carried out to justify the calculated solubility in this study. By adopting the same interaction parameters, calculations were also made using the formulation of Nishizawa and co-workers to compare the difference between both theoretical treatments of magnetic free energy [8, 10].

0953-8984/90/265787 + 10 $03.50

2. Expression of Gibbs free energy

It has been shown [1–4, 7] that the Gibbs free energy of a solution is separable into non-magnetic and magnetic terms, namely

$$G = [G]_{NM} + [G]_{Mag}. \tag{1}$$

In the case of the Co–Cu system, the non-magnetic component of the Gibbs free energy is described as follows, using a subregular solution model:

$$[G]_{NM} = [{}^0G_{Co}]_{NM}(1 - X_{Cu}) + [{}^0G_{Cu}]_{NM}X_{Cu} + {}^{id}G + {}^{ex}G_{NM} \tag{2}$$

where X_{Cu} is the mole fraction of Cu, and ${}^{id}G$ and ${}^{ex}G_{NM}$ are the ideal mixing energy and the excess mixing energy, respectively. The non-magnetic free energy relative to the mechanical mixture of components Co and Cu in the equilibrium state is

$$\begin{aligned}\Delta G_{NM} &= {}^{id}G + {}^{ex}G_{NM} \\ &= RT[(1 - X_{Cu})\ln(1 - X_{Cu}) + X_{Cu}\ln X_{Cu}] \\ &\quad + X_{Cu}(1 - X_{Cu})[A + B(1 - 2X_{Cu})]\end{aligned} \tag{3}$$

where A and B are the interaction parameters in a subregular solution and R is the gas constant.

The magnetic free energy can be written as

$$G_{Mag} = [{}^0G_{Co}]_{Mag}(1 - X_{Cu}) + [{}^0G_{Cu}]_{Mag}X_{Cu} + {}^{ex}G_{Mag} \tag{4}$$

where ${}^{ex}G_{Mag}$ is the magnetic free energy relative to the mixture of components Co and Cu in the equilibrium magnetic state. For a phase diagram calculation, it is convenient to use the completely paramagnetic standard state, as was done in previous papers [8, 11, 12], because the experimental data at higher temperatures (especially at temperatures much higher than the Curie temperature) are more trustworthy than those at lower temperatures. Thus the magnetic free energy is reformulated as

$$G_{Mag} = [{}^0G_{Co}]_{Mag}(1 - X_{Cu}) + [{}^0G_{Cu}]_{Mag}X_{Cu} + {}^{ex}G^{cpm\rightarrow eqm} \tag{5}$$

where ${}^{ex}G^{cpm\rightarrow eqm}$ is the magnetic excess free energy of the equilibrium state relative to the mixture of components Co and Cu in the completely paramagnetic state. The total free energy of mixing relative to the completely paramagnetic state is as follows:

$$\begin{aligned}\Delta G &= RT[(1 - X_{Cu})\ln(1 - X_X) + X_X\ln X_X] \\ &\quad + X_{Cu}(1 - X_{Cu})[A + B(1 - 2X_{Cu})] + {}^{ex}G^{cpm\rightarrow eqm}.\end{aligned} \tag{6}$$

According to Chuang *et al* [10], the magnetic free energies are expressed by the following equations:

$${}^{ex}G^{cpm\rightarrow eqm} = \begin{cases} -[K_pT_C/(8p)^2]\exp[8(1 - T/T_C)] & T \geqslant T_C \quad (7) \\ -[K_pT_C/(8p)^2](1 + 8p) + (K_f/4 + K_p/8p)T & \\ \quad -(K_fT_C/16)\{3 + \exp[-4(1 - T/T_C)]\} & T \leqslant T_C \quad (8) \end{cases}$$

with $p = 2$ for the FCC lattice. The quantities K_f and K_p are related to the saturation magnetisation of the alloys as

$$K_f = \{4(1 - f_s)/[1 - \exp(-4)]\}CR\ln(\beta + 1) \tag{9}$$

$$K_p = 8f_sCR\ln(\beta + 1) \tag{10}$$

where $f_s = 0.105$ for the FCC lattice [10], C is the empirical factor and β is the mean magnetic moment per atom. T_C, C and β are expressed as linear functions of the concentration X_{Cu}:

$$T_C = 1394 - 747X_{Cu} \tag{11}$$

$$C = (1 - X_{Cu})C_{Co} + X_{Cu}C_{Cu} \tag{12}$$

$$\beta = (1 - X_{Cu})\beta_{Co} + X_{Cu}\beta_{Cu}. \tag{13}$$

In this study, C_{Cu} is taken as unity and β_{Cu} as zero. The magnetic moment β_{Co} of Co, is taken as 1.75 and C_{Co} as 0.634 [10].

3. Calculation of mutual solubility in the Co–Cu binary system

The criteria for the phase equilibrium between α-Co and ε-Cu are given as

$$\mu^{\alpha}_{Co} = \mu^{\varepsilon}_{Co} \tag{14a}$$

$$\mu^{\alpha}_{Cu} = \mu^{\varepsilon}_{Cu}. \tag{14b}$$

The chemical potentials can be obtained from equation (6). For the calculation of mutual solubility, we use the same function to represent the Gibbs free energy of α-Co and ε-Cu phases with the same crystal structure. The criteria for equilibrium can be reformulated as

$$\mu_{Co}(X_{Cu,1}) = \mu_{Co}(X_{Cu,2}) \tag{15a}$$

$$\mu_{Cu}(X_{Cu,1}) = \mu_{Cu}(X_{Cu,2}). \tag{15b}$$

The concentrations $X_{Cu,1}$ and $X_{Cu,2}$ of mutual solubility in the Co–Cu alloy and the interaction parameters A and B can be obtained from the above equations with two variables known at a fixed temperature.

4. Experimental procedures

The Co–Cu alloys with 2, 5, 7.5, 8.5, 10 and 12 at.% Cu were prepared by arc melting in a cold copper hearth under an argon atmosphere. After melting, the alloys were sealed in evacuated quartz tubes and heat treated by the following procedures:

(i) homogenisation and solution treatment at 1403 K for 168 h, followed by brine quenching by breaking the quartz tubes;

(ii) isothermal aging under argon protection at 1273, 1313, 1333 or 1373 K for 2 h.

The samples were then studied by x-ray diffractometry (XRD) to measure the lattice constant which is a function of the solute concentration X_{Cu}. The XRD patterns were obtained from a diffractometer with filtered monochromatic Cu Kα_1 radiation at 45 kV and 25 mA, using a step-scan method with a sampling width of 0.002°. 'Primary' lattice constants were calculated using the {111}, {200} and {311} diffractions from the Miller indices and measured angles. The calculated values were plotted against the function $f = (\cos^2\theta)/\theta + (\cos^2\theta)/\sin\theta$ and then extrapolated to $f = 0$ ($2\theta = 180°$), where a precise lattice constant was obtained. A silicon powder was incorporated in the sample to correct the device errors in diffraction peaks.

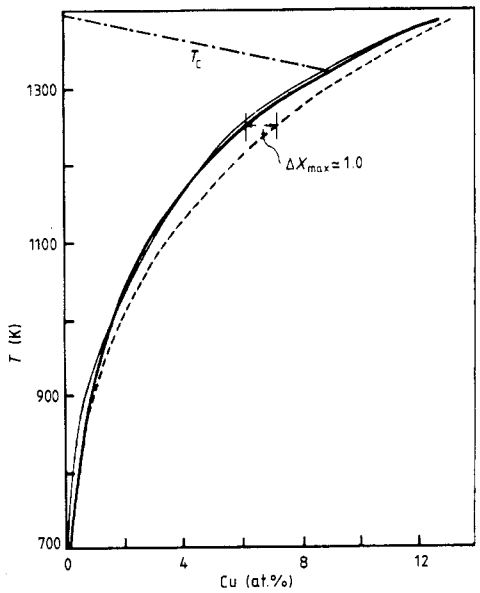

Figure 1. The calculated Cu solubility (——, this work; – – –. this work, no G_{Mag}) and those from [13] (——) in α-Co of the Co–Cu system.

The samples were also examined using a superconducting quantum interference device (SQUID) to measure the magnitude of the intrinsic coercivity and then to confirm the precipitation of the Cu-rich phase. The heat-treated samples were cut to rods with a length-to-width ratio of greater than 10 with a slow-speed diamond saw cutter and then stress relieved at 473 K. To detect the coercivity, the rod samples were first magnetised under a 30 000 G field, followed by demagnetisation and reverse magnetisation.

5. Results and discussion

5.1. Mutual solubility calculation

The coefficients A_1, A_2, B_1 and B_2 of the interaction parameters A and B in equation (3) were taken as linear functions of temperature:

$$A = A_1 + A_2 T \tag{16a}$$

$$B = B_1 + B_2 T. \tag{16b}$$

These coefficients were evaluated by means of a linear regression, using the concentration values of mutual solubilities taken from the high-temperature portion (temperature higher than the Curie temperature) of the phase diagram [13]. The coefficients thus obtained are as follows:

$$A = 48570 - 12.60T \tag{17a}$$

$$B = -4721 + 1.845T. \tag{17b}$$

The copper solubility in an α-Co solid solution of the Co–Cu system was calculated by considering the magnetic free energy using equations (6) and (7) and is shown in figure 1. Figures 2 and 3 show the Arrhenius plots of the solid state mutual solubility.

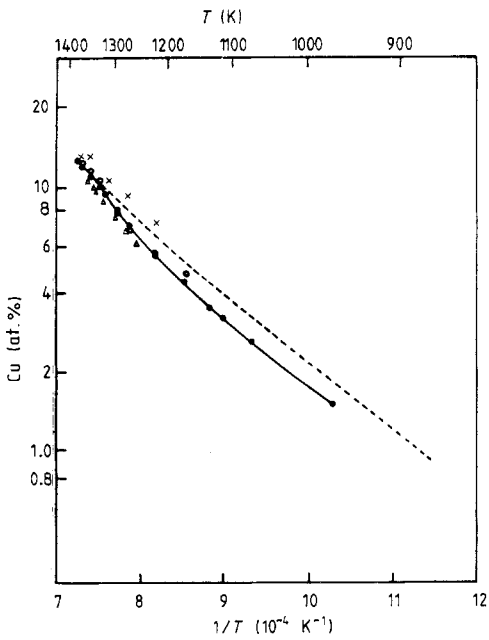

Figure 2. The Arrhenius plot of the calculated Cu solubility (●) and those listed in [13] (○, [8]; △, [14]; ×, [15]) in α-Co of the Co–Cu system.

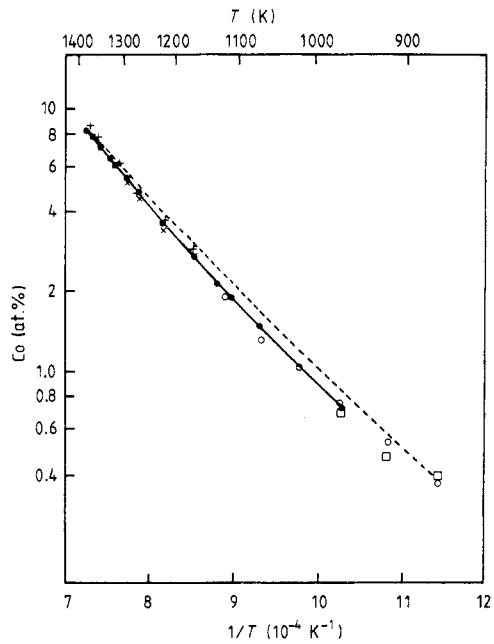

Figure 3. The Arrhenius plot of the calculated Co solubility (●) and those listed in [13] (×, [8]; +, [15]; □, [16]; ○[17]) in ε-Cu of the Co–Cu system.

Assuming that the alloys were all in a hypothetical, completely paramagnetic state throughout the target temperature range, the mutual solubility obtained by removing the magnetic free energy are shown as broken curves in figures 1–3 from the results of other investigators [13].

It is obvious that the relation between solubility calculated by considering the magnetic free energy and temperature no longer obeys the Arrhenius equation at temperatures near the Curie temperature. Such an anomaly is manifestly due to the magnetic transition which is as significant in this study as that observed by Nishizawa and coworkers, who used different formulation for the magnetic free energy. The mutual solubility is lowered because of the introduction of the magnetic free energy. This is shown in figure 1 as a solvus line protruding towards the Co-rich end, with respect to the line (broken curve) obtained by neglecting the magnetic free energy.

Figure 4 shows the ΔG versus X curves of the Co–Cu system at 1323 K. The magnetic free energy ${}^{ex}G_{mag}$ is the largest at an infinitely small amount of Cu and is reduced by the addition of Cu, as shown in figure 4(*a*). Figure 4(*b*) shows the effect of incorporating ΔG_{mag} into ΔG_{NM}, leading to a decreased total Gibbs free energy ΔG_t. It is obvious that the effect of adding Cu is great at low concentrations, leading to a reduced mutual solubility at the Co-rich end. It can be negligible at high Cu concentrations, e.g. for $X_{Cu} > 0.3$. This is typical of ferromagnetic M–X binary alloys (M represents a ferromagnetic element and X a non-magnetic element).

The magnetic moment and Curie temperature of the ferromagnetic element M are altered by the amount of solid solution of the non-magnetic element X. These two factors should be taken into account in discussing the influence of the non-magnetic element on

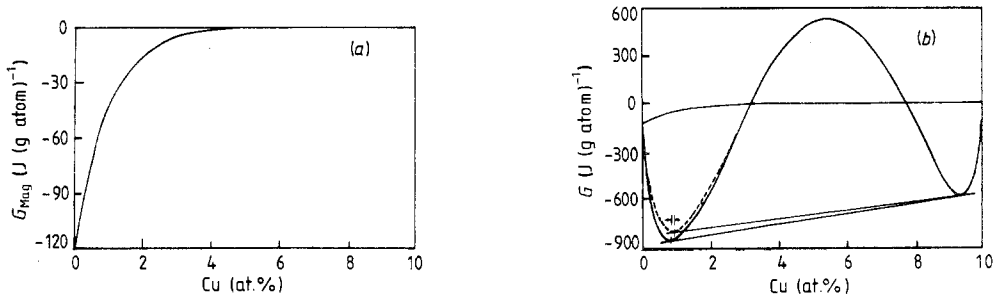

Figure 4. The ΔG versus X curves of the Co–Cu system at 1323 K: (*a*) the dependence of magnetic free energy on the Cu concentration; (*b*) total free energy G_t (——), magnetic free energy G_{Mag} (——) and non-magnetic free energy G_{Nm} (– – –).

the magnetic free energy. Chang *et al* [10] considered the magnetic free energy of the solid solution to be similar to that of the pure ferromagnetic element (equation (6)) except for the solute concentration dependence of the magnetic entropy, the magnetic moment β, the constant C and the Curie temperature T_C, as listed in equations (8)–(12). The influence of the non-magnetic element on the magnetic free energy is then correlated quantitatively to β, C and T_C.

The ferromagnetic free energy relative to the fully uncoupled magnetic spin state (i.e. completely paramagnetic state) can be treated differently, as in [8]:

$$^{ex}G_{Mag} = (1 - m_X X_X)\,{}^0G(T')_{M,Mag} \tag{18a}$$

$$T' = T - \Delta T_X X_X \tag{18b}$$

where ΔT_X is the slope of the Curie temperature in the M–X solid solution. $^{ex}G_{Mag}$ is taken as zero at temperatures much higher than T_C. $^0G(T')_{M,Mag}$ in equation (18*a*) is the modified magnetic free energy corresponding to the Curie temperature change. The influence of the non-magnetic element on the magnitude of the magnetic free energy is described by m_X in equation (18*a*), which must be evaluated from the concentration dependence of the magnetic entropy in the M–X solid solution. Since the values of m_X are still unknown because of the lack of sufficient experimental data, they are, for simplicity, taken as zero for the non-magnetic element and unity for the magnetic element.

The solubilities calculated by incorporating magnetic free energy into total free energy using the above two thermodynamic treatments have very similar values and asymmetric characteristics. This arises from the same considerations of concentration dependence and subregular solution model. It is also worthwhile to note that, although the solubility obtained with treatment used by Chuang *et al* is slightly higher than that obtained with the treatment used by Nishizawa and co-workers because of the different treatments of the concentration dependency, this difference is very small and can even be negligible. However, the formulation of magnetic free energy by Chuang *et al* seems to be thermodynamically more rational and more easily realised than that of Nishizawa and co-workers. Nevertheless, the latter is simpler for computer calculation. In this study, calculation of the mutual solubility (miscibility gap) of the Co–Cu system, considering the magnetic free energy with the interaction parameter coefficients obtained by Nishizawa *et al* [18], was also carried out, where

$$A = 49400 - 13.26T \tag{19a}$$

$$B = -3675 + 1.03T. \tag{19b}$$

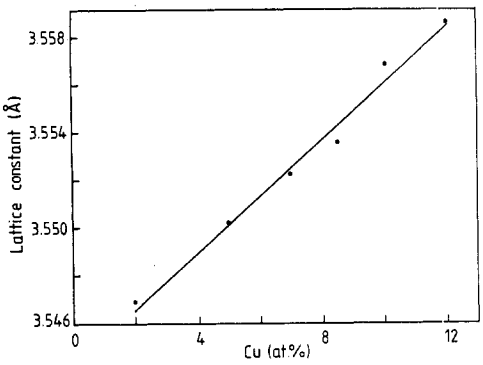

Figure 5. The Vegard plot showing the lattice constant of FCC Co–Cu solutions at 298 K, measured from the quenched samples aged at 1373 K.

The calculated solubility is approximately the same as that calculated with the coefficients obtained in this study.

5.2. Determination of solubility by experiments

The copper concentrations of the Co–Cu alloys in this study were between 2 and 12 at.%. The lattice constant measurement was made on the quenched sample after isothermal aging at temperatures ranging from 1173 to 1373 K. The lattice constant of each sample depends on the solubility. Figure 5 shows that the lattice constant is approximately a linear function of copper concentration in the Co–Cu alloys. The relation obeys Vegard's rule as evidenced from the measured data of the solution-treated single-phase alloys in the present work. The solubility limit was determined by converting the measured lattice constant of each alloy to the solute concentration by using the Vegard plot (figure 5).

The measured lattice constants and the corresponding solute concentrations are shown in table 1 with the thermodynamically calculated solubilities for comparison. The solubilities of the quenched alloys approximately coincide with the calculated values, although deviation is quite large owing to the limited precision of our x-ray facility.

The intrinsic coercivity H_{ci} of the alloys is a structure-sensitive property. The intrinsic coercivity of a single-phase ferromagnetic Co–Cu alloy is greatly increased by the precipitation of a second phase and this enables verification of the calculated solvus to be made. The intrinsic coercivity of the quenched samples is listed in table 2. For comparison, the thermodynamically calculated solubilities are also shown in table 2. It is obvious that the intrinsic coercivity of the samples quenched from the two-phase region is several times higher than those from the single-phase region of the α-Co solid solution. The experimental results of coercivity measurement agree well with the calculated solvus curve. There is an anomaly that the coercivity of the 10 at.% Cu alloy aged at 1333 K is greater than that of the same alloy aged at 1313 K, while the proportion of the second phase in the latter sample should be greater. This was probably due to two possibilities:

(i) higher residual stress in the former due to cutting;

(ii) the precipitates in the latter case which might grow much larger owing to earlier nucleation (arising from greater undercooling) compared with the former, and hence a lower pinning force on the domain wall in the latter case.

Table 1. The lattice constants and the Cu solubilities in α-Co for the alloys aged at 1273, 1313, 1333 and 1373 K. The Cu solubilities are converted from the measured lattice constants by the relation shown in figure 5, as $a = 3.5543 + 0.0012$ at.% Cu.

Aging temperature (K)	Lattice constant; Cu solubility (at.%) for the following alloy Cu contents						Maximum Cu solubility	
	2.0 at.%	5.0 at.%	7.5 at.%	8.5 at.%	10.0 at.%	12.0 at.%	Calculated	[8]
1373	3.5469; 2.2	3.5502; 5.0	3.5522; 6.7	3.5535; 7.8	3.5568; 10.6	3.5585; 12.1	12.0	12.3
1333	—; —	—; —	3.5528; 7.2	3.5539; 8.2	3.5555; 9.6	3.5563; 10.2	10.0	10.6
1313	—; —	3.5504; 5.2	3.5524; 6.9	3.5538; 8.1	3.5545; 8.7	3.5551; 9.2	8.9	—
1273	—; —	3.5497; 4.6	3.5524; 6.9	—; —	—; —	—; —	7.1	6.9

Table 2. The intrinsic coercivity H_{ci} of the alloys aged at 1333 and 1313 K.

Aging temperature (K)	Intrinsic coercivity (Oe) for the following alloy Cu contents			Calculated Cu solubility (at.%)
	7.5 at.%	8.5 at.%	10.0 at.%	
1333	11.5	18.0	45.0	10.0
1313	13.5	21.0	38.5	8.9

6. Conclusions

The Co-rich end solvus of the Co–Cu binary system was recalculated by taking into account the effect of copper on the magnetic free energy. It was found that the solubility of copper in α-Co is lowered as manifested by the anomaly of the calculated Arrhenius plot. The results calculated using the treatments of Nishizawa and co-workers and of Chuang *et al* of magnetic free energy (using the same interaction parameters) led to similar asymmetric properties of mutual solubilities. However, the calculated solubility with the theoretical treatment of Chuang *et al* is slightly higher than that obtained with the treatment of Nishizawa and co-workers. The calculated solubility was also verified using a lattice constant determination by XRD and intrinsic coercivity measurement by SQUID.

Acknowledgment

This work has been supported by the National Science Council of the Republic of China under contract NSC 78-0405-E006-21R.

References

[1] Zener C 1955 *Trans. AIME* **203** 619
[2] Weiss R J and Tauer K J 1956 *Phys. Rev.* **102** 1490
[3] Hofmann J A, Paskin A, Tauer K J and Weiss R J 1956 *Phys. Chem. Solids* **1** 45
[4] Kaufmann L, Clougherty E V and Weiss R J 1963 *Acta Metall.* **11** 323
[5] Hillert M, Wada T and Wada H J 1967 *J. Iron Steel Inst.* **205** 539
[6] Harvig H, Kirchner G and Hillert M 1972 *Metall. Trans.* **3** 329
[7] Nishizawa T, Hasebe M and Ko M 1979 *Acta Metall.* **27** 817
[8] Hasebe M and Nishizawa T 1980 *Calphad* **4** 83
[9] Hillert M and Jarl M 1978 *Calphad* **2** 227
[10] Chuang Y Y, Schmid R and Chang Y A 1985 *Metall. Trans.* A **16** 153
[11] Chuang Y Y, Schmid R and Chang Y A 1984 *Metall. Trans.* A **15** 1921
[12] Chuang Y Y, Lin Y and Chang Y A 1987 *Calphad* **11** 57
[13] Nishizawa T and Ishida K 1984 *Bull. Alloy Phase Diagrams* **5** 161
[14] Bruni F J and Christian J W 1972 *Mater. Sci. Eng.* **9** 241
[15] Old C F and Haworth C W 1966 *J. Inst. Met.* **94** 303
[16] Knappwost A 1957 *Z. Phys. Chem.* **12** 30
[17] Livingston J D 1959 *TMS-AIME* **215** 566
[18] Hasebe M, Oikawa K and Nishizawa T 1982 *J. Japan. Inst. Met.* **46** 584